JOURNAL OF GEOPHYSICAL RESEARCH, VOL. 100, NO. D9, PAGES 18,727–18,737, SEPTEMBER 20, 1995

Inertio-gravity wave parameter estimation from cross-spectral analysis

John Y. N. Cho
Arecibo Observatory, Arecibo, Puerto Rico

Abstract. We outline a method for extracting inertio-gravity wave parameters using the autospectra and cross spectra of the horizontal perturbation winds. In essence, we define a statistical hodograph for each spectral bin, thus combining the advantages of the rotary spectrum and hodograph methods. Furthermore, we include the effects of the background vertical shear in the parameter estimation equations, a step that had often been omitted in the past. Applying this technique to a long-period data set taken with the Arecibo 430-MHz radar, we explore its usefulness as well as its limitations. Our analysis of this data set also supports the interpretation of horizontal wind-perturbation rotation in the lower stratosphere over Arecibo as inertio-gravity waves rather than mountain waves imbedded within a background vertical shear.

Introduction

Due to their short vertical wavelengths and long time periods, stratospheric inertio-gravity waves (IGWs) have been relatively difficult to observe, requiring fine vertical resolution of the order of hundreds of meters and continuous monitoring over a period of several days. Early studies of IGWs were based on balloon-based radiosonde data [*Thompson*, 1978]. More recently, the maturation of stratosphere-troposphere (ST) radars has provided us with high-resolution, long-period wind measurements without the space-time ambiguity problem associated with the slow ascent and the horizontal drift of balloons. Although the radar measurements also have their own ambiguities (e.g., spatially separated line-of-sight velocity conversion to a single-point horizontal velocity for the Doppler beam swinging method), they have contributed significantly to the advancement of IGW studies in recent years [*Cornish and Larsen*, 1989; *Thomas et al.*, 1992; *Sato*, 1994].

Because the observations so far have been single-location Eulerian, basic wave parameters such as horizontal wavelength and intrinsic period have been inferred from the polarization of the perturbation velocity. The two wave-parameter extraction methods commonly used are (1) the rotary spectrum and (2) the hodograph. Each method has its own advantages and disadvantages. In this paper we introduce a third approach to the problem of IGW parameter estimation, the cross spectrum, which combines the strengths of the previous two methods. (It turns out that the cross-spectral approach is essentially equivalent to the Stokes parameter method proposed by *Vincent and Fritts* [1987].)

We then apply the cross-spectral method to the tropospheric and stratospheric wind data taken with the Arecibo 430-MHz radar during the 1989 Arecibo initiative in dynamics of the atmosphere (AIDA) campaign. AIDA was primarily an experiment to compare mesospheric winds measured by different instruments; however, the investigators had the foresight to run a "piggyback" program on the main radar that recorded winds in the upper troposphere and lower stratosphere. Because the time-competitive Arecibo system is rarely allocated such long, continuous blocks of time, the result is the best Arecibo data set yet for studying IGWs.

The availability of the AIDA data is also important because there is some controversy over the interpretation of the previous stratospheric, long-period, short-vertical-wavelength, elliptically polarized Arecibo wind perturbation data as IGWs. *Hines* [1989] filed a dissent against the Arecibo IGW interpretation of *Maekawa et al.* [1984], claiming that mountain waves with much shorter intrinsic periods could, in the presence of vertical shear in the background horizontal winds, appear to be very much like IGWs, especially in the elliptical polarization of the perturbation winds that are usually taken to be a manifestation of IGWs. And, by extension, *Hines* [1989] cast a doubt on all other previous observations of stratospheric IGWs, since none had taken into account the vertical shear factor. In response, *Cornish and Larsen* [1989] have interpreted 1982 Arecibo data as IGWs, and *Sato* [1994] has taken into account the vertical shear factor in analyzing middle and upper atmosphere (MU) radar data for IGWs.

Thus our purpose in this paper is to (1) introduce the cross-spectral method for IGW analysis, (2) test its effectiveness with the AIDA data set, and (3) establish whether there are real IGWs in the stratosphere over Arecibo.

Paper number 95JD01752.
0148-0227/95/95JD-01752$05.00

The Cross-Spectral Method

Spectral Processing

Since the polarization of the perturbation wind vector is the key to extracting IGW parameters, two methods have been commonly used in the past to analyze the polarization. The first method, the rotary spectrum, was first applied to geophysical fluid data by *Gonella* [1972] and to atmospheric IGWs by *Thompson* [1978]. This method takes the complex Fourier transform of $u + iv$, where u and v are the zonal and meriodional components of the horizontal perturbation wind, and yields the clockwise (CW) rotational power in the negative spectrum and the counterclockwise (CCW) rotational power in the positive spectrum. Since the sense of horizontal perturbation wind rotation with height indicates the vertical direction of IGW energy propagation (cyclonic, downward; anticyclonic, upward), the rotary-spectral method provides the following information sorted by the absolute value bin of the vertical wavenumber spectrum: (1) the likely presence of an IGW as indicated by a difference of power in the cyclonic and anticyclonic components (equal levels would indicate linear polarization, which would imply random fluctuations or a pure gravity wave uninfluenced by the Coriolis effect (but note the objection of *Hines* [1989] mentioned above)) and (2) the vertical sense of IGW energy propagation.

The second method, the hodograph, is a standard tool in meteorology. It was first applied to oceanic inertial oscillations by *Kundu* [1976] and to atmospheric IGWs by *Cot and Barat* [1986]. The idea is to trace the tip of the horizontal wind vector with respect to height. If enough points are taken to span one wavelength or one observed period of an IGW, then an ellipse should be inscribed. The following parameters can then be extracted: (1) the vertical sense of IGW propagation from the rotational sense, (2) the line of horizontal propagation that is parallel to the major axis of the ellipse, and (3) the intrinsic wave frequency, ω, which is calculated from the ratio of the major to the minor axis of the ellipse.

Each method has its disadvantages. The rotary spectrum fails to yield the horizontal propagation direction and the intrinsic frequency, ω. The hodograph, on the other hand, cannot sort out the results with respect to the vertical wavelength, m; one has to hope for a monochromatic wave or filter the input data according to some a priori criteria. *Eckermann and Hocking* [1989] warn that wave parameters extracted with the hodograph are not accurate if there are multiple waves present.

The cross-spectral method combines the advantages of the rotary-spectral and hodograph methods. (However, there is another price to pay as we shall see later.) We note that it is, in principle, equivalent to the Stokes parameter method proposed by *Vincent and Fritts* [1987] and applied by *Eckermann and Vincent* [1989]. Also, all of the methods discussed here can be examined under the general space-time spectral analysis formulation of *Hayashi* [1979].

Here is an outline of the cross-spectral method:

1. Fourier transform u and v with respect to altitude or time.

2. Form the autospectra and cross spectra. The cross spectrum is given by

$$S_{UV}(\xi) = \frac{< U(\xi)V^*(\xi) >}{< |U(\xi)|^2 >^{\frac{1}{2}} < |V(\xi)|^2 >^{\frac{1}{2}}} \qquad (1)$$

where U and V are the Fourier transforms of u and v; ξ is the independent variable in the transformed domain (either m or the observed frequency, ω_0, in this case). Note that the ensemble averaging denoted by the brackets means that the cross spectrum requires averaging over altitude or time; this additional ambiguity in space-time is the price one pays for using this approach. Note also that the autospectra should be normalized to be amplitude rather than power.

3. Form the coherence, $C_{UV}(\xi)$, which is the magnitude of $S_{UV}(\xi)$, and $\Phi_{UV}(\xi)$, which is the phase of $S_{UV}(\xi)$.

The coherence, which varies from 0 to 1, gives a measure of the correlation between U and V in a given spectral bin. Thus it is a good indicator for the presence of wave energy in that spectral bin. Even if the autospectra do not have noticeable peaks, a significant peak in the coherence shows that for that particular spectral bin, u and v were varying in some nonrandom manner indicating a wave motion.

The sign of the phase yields the sense of wind rotation for a given spectral bin. For the definition of the cross spectrum given in (1), positive phase means CW and negative phase means CCW. Then for spectra taken with respect to height in the northern hemisphere, positive phase corresponds to upward energy propagation, and negative phase corresponds to downward energy propagation. For spectra taken with respect to time in the northern hemisphere, IGWs should exhibit positive phases (anticyclonic rotation) when the observed and intrinsic wave frequencies have the same sign; if the Doppler shift if great enough to reverse the sign relation between the observerd and intrinsic frequencies, then the IGWs would have negative phases (cyclonic rotation). The magnitude of the phase yields the type of polarization: 0° and 180° correspond to linear (pure gravity waves, unless the propagation direction is exactly zonal or meridional) and all other values to elliptical (IGWs), with the special case of a perfectly circular polarization corresponding to pure inertial oscillation.

The autospectra by themselves yield the energy content in U and V per given spectral bin but are not as good indicators of the presence of wave motion as the coherence. However, the amplitudes of the autospectra in combination with the phase of the cross spectrum define an ellipse for a given spectral bin. Therefore it is as if a series of hodographs are created and sorted according to the spectral bins.

One can immediately see the advantages of the cross-spectral method. Like the rotary-spectral approach the information is sorted according to the bins in the Fourier transform domain, so there is no need to perform an a priori filtering of the data as required for hodographs. On the other hand, the output of the cross-spectral method yields just as much information as a hodograph. In addition, we gain a measuring stick for the presence of waves called the cross-spectral coherence.

The disadvantage, as mentioned earlier, is the need to average in the wavenumber or frequency domain in order to form the cross spectrum. At first glance this may not seem like a high price to pay, but we will see that it has important implications in the extraction of wave parameters.

Wave-Parameter Estimation

We wish now to estimate ω, k (horizontal wave number), and, if the Fourier transform is taken with respect to time, m of the wave. Note that the wave-parameter extraction process is not a unique feature of the cross-spectral method; once the polarization ellipse has been defined, either by hodograph or cross spectra, the following steps can be applied to estimate the wave parameters. In order to proceed, we need the following three relations. The polarization relation is given by

$$R = \left| \frac{f}{\omega} - \frac{k}{m\omega} \frac{\partial \bar{v}}{\partial z} \right| \tag{2}$$

where R is the magnitude of the ratio of the minor to the major axis of the polarization ellipse, f is the Coriolis parameter, and z is the altitude variable. Note that we have chosen the coordinate system such that $\bar{u}$ is the mean background horizontal wind component that is in the same direction as the horizontal wave vector, $\mathbf{k}$; thus $\bar{v}$ is the mean horizontal wind component perpendicular to the wave propagation. The dispersion relation, assuming $k^2 \ll m^2$ and $2\pi/m \ll H$, where H is the atmospheric scale height, is given by

$$\omega^2 = f^2 + \frac{N^2 k^2}{m^2} - \frac{2fk}{m} \frac{\partial \bar{v}}{\partial z} \tag{3}$$

where N is the angular Brunt-Väisälä frequency. Note that we have included the effects of vertical shear in the background wind field as manifested by the $\partial\bar{v}/\partial z$ terms in both (2) and (3), following the work of *Kunze* [1985] and *Sato* [1994]. Finally, the Doppler relation is given by

$$\omega_0 = \omega + \bar{u}k \tag{4}$$

For a given location, f is a constant (the value over the Arecibo Observatory is 4.6×10^{-5} rad s^{-1}). The mean horizontal wind is calculated from the input data. The horizontal wave vector is parallel to the major axis of the wind perturbation ellipse; this information is used to form $\bar{u}$ and $\bar{v}$. N can be calculated from temperature profile measurements (we will use measurements from balloon-launched radiosondes); otherwise, a mean profile from a standard atmosphere table could be used.

If the spectra are taken with respect to time, then R and ω_0 are the givens; (2), (3), and (4) are required to solve for ω, k, and m. The horizontal wave propagation direction is parallel to the major axis of the wind perturbation ellipse. If the spectra are taken with respect to altitude, then R and m are the givens; only (2) and (3) are needed to solve for ω and k.

Solving for ω we get

$$\omega = \frac{fR\left|N^2 - \left(\frac{\partial \bar{v}}{\partial z}\right)^2\right|}{N^2R^2 - \left(\frac{\partial \bar{v}}{\partial z}\right)^2} + \frac{f\left|\frac{\partial \bar{v}}{\partial z}\right| \left\{\left|N^2 - \left(\frac{\partial \bar{v}}{\partial z}\right)^2\right| (1-R^2)\right\}^{\frac{1}{2}}}{N^2R^2 - \left(\frac{\partial \bar{v}}{\partial z}\right)^2} \tag{5}$$

such that the intrinsic wave frequency can be calculated from only the measured quantities. Now the other parameters can be expressed in terms of ω.

For the case of m spectra, the horizontal wavenumber is given by

$$k = \frac{fm}{N^2} \frac{\partial \bar{v}}{\partial z} \pm \frac{m}{N} \left[\frac{f^2}{N^2} \left(\frac{\partial \bar{v}}{\partial z} \right)^2 + \omega^2 - f^2 \right]^{\frac{1}{2}} \tag{6}$$

For the case of ω_0 spectra,

$$k = \frac{\omega_0 - \omega}{\bar{u}} \tag{7}$$

and

$$m = \frac{fk}{f^2 - \omega^2} \frac{\partial \bar{v}}{\partial z} \pm k \left[\left(\frac{f}{\omega^2 - f^2} \frac{\partial \bar{v}}{\partial z} \right)^2 + \frac{N^2}{\omega^2 - f^2} \right]^{\frac{1}{2}} \tag{8}$$

The group velocity can then be calculated from the dispersion relation; the horizontal component is

$$v_{gh} = \frac{N^2 k}{\omega m^2} - \frac{f}{\omega m} \frac{\partial \bar{v}}{\partial z} \tag{9}$$

and the vertical component is

$$v_{gz} = -\frac{N^2 k^2}{\omega m^3} + \frac{fk}{\omega m^2} \frac{\partial \bar{v}}{\partial z} \tag{10}$$

The horizontal and vertical components of the phase velocity are, of course, $v_{ph} = \omega/k$ and $v_{pz} = \omega/m$.

Unfortunately, we need one more relation to resolve the sign ambiguity in the two roots of (6) and (8). An equation that includes the vertical velocity perturbation can be used for radar data that include the vertical velocity; however, since the vertical velocity was not measured during AIDA, we shall instead use the relation between temperature perturbation, T, and v [*Sato and Yamada*, 1994],

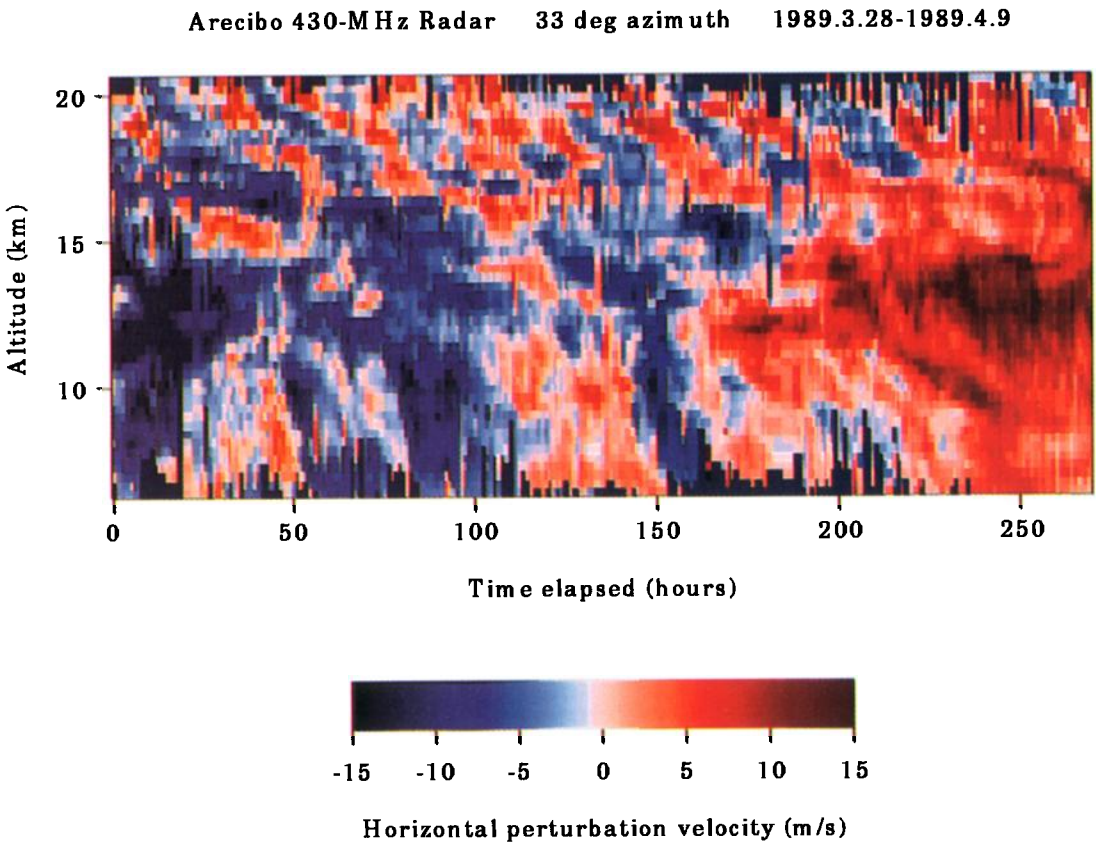

Plate 1. The perturbation horizontal wind at 33° E of N during Scene 2. 0 hour corresponds to 1989-3-28, 2200 UT. The gaps (shown in black) in the top ranges are due to lack of signal, and the gaps in the bottom ranges are due to the combination of strong ground clutter and low wind speeds.

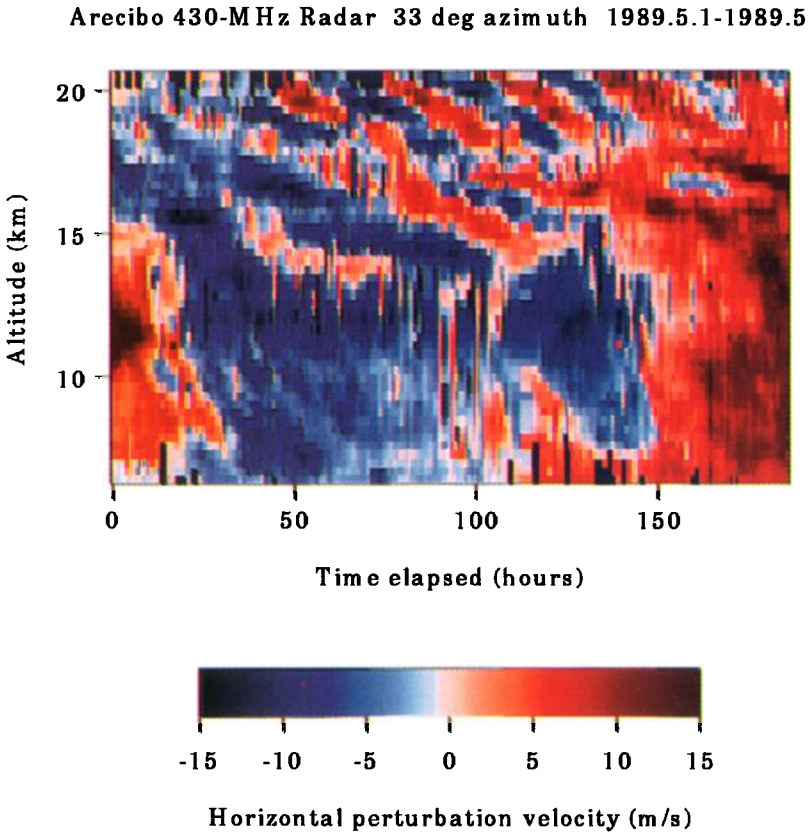

Plate 2. Same as Plate 1 but with data from Scene 3. The 0 hour corresponds to May 5, 1989, 2100 UT.

$$\frac{T}{\bar{T}} = \frac{-N^2 kv}{g\left(fm - k\frac{\partial \bar{v}}{\partial z}\right)} \tag{11}$$

where $\bar{T}$ is the background temperature and g is the gravitational acceleration. The temperature measurements were made by balloon-based rawinsondes that were launched from San Juan (80 km east of Arecibo) every 6 hours during Scene 2 of AIDA and every 12 hours during other times.

A potential problem with the cross-spectral wave parameter estimation method is that the background wind and temperature fields may vary nonnegligibly inside the altitude-time space within which the spectra are taken and averaged. The larger the variability is the greater the uncertainty of the estimated parameters will be. Thus in the next section we will explore the sensitivity of the method to real data.

Application of the Cross-Spectral Method to Real Data

The 1989 AIDA Experiment

The main purpose of the AIDA experiment was to clarify what type of motions the MF/HF partial-reflection radar technique was measuring in the lower ionosphere. Since an incoherent scatter radar was believed to measure the true wind velocity, a 3.2-MHz partial-reflection system was set up near the Arecibo Observatory in order to make comparative observations with the Arecibo 430-MHz radar. Optical instruments were also used for wind measurements, and density measurements in the stratosphere were made with a lidar [*Meriwether*, 1993]. For a summary of the campaign see *Hines et al.* [1993].

Unusually long time periods (for the time-competitive Arecibo system) were reserved for the AIDA experiment. To take advantage of this opportunity, the organizers ran a stratospheric-tropospheric observation program on the 430-MHz system whenever possible. Consequently, we have available fairly long data sets that are quite suitable for studying IGWs.

There were three "scenes" in AIDA, Act 1989. Scene 1 was March 7-15, 1989, Scene 2 was March 28 to April 11, and Scene 3 was May 1-9. In this paper we will examine data from the two longest segments: Scenes 2 and 3. Because of a long data gap on 4/9, we will only take 3/28 to 4/9 for Scene 2.

The Arecibo 430-MHz system used as an ST radar is described by *Woodman* [1980]. It is located at 18.3° N, 66.8° W with a corresponding inertial period of 38.2 hours. During AIDA the radar was operated with an effective interpulse period of 1.7 ms, a pulse length and sampling gatewidth of 300 m, and the data sampling window between 6 and 21 km in altitude. During Scenes 2 and 3, 12 coherent integrations were performed on-line and the antenna beam was fixed in zenith angle at 11° and scanned in azimuth angle in the following approximate pattern: 1.5 hours at 33°, 10 min at 303°, 10 min at 213°, 20 min at 123°, 10 min at 213°, and 10 min at 303°, then repeat (0° is north and the numbers increase clockwise); the pattern is not optimal for inferring vector winds: it was a compromise with the ionospheric data acquisition mode that was interleaved throughout.

In the off-line data processing, 128-point fast Fourier transforms (FFTs) were taken, 23 spectra were averaged with half-segment overlap (moving average), and a nonlinear least squares routine was used to fit to the spectra and extract the Doppler velocities (a procedure similar to the one developed by *Sato and Woodman* [1982] to overcome the severe ground clutter problem at Arecibo). The line-of-sight velocities were then averaged over one azimuth scan, collapsed to the two orthogonal directions, 33° and 123°, and converted to horizontal speeds assuming negligible vertical velocity contamination (not a bad assumption during periods of little convective activity such as this one).

The bottom line is that we have horizontal winds in two orthogonal directions with 0.7-m s^{-1} resolution, between 6.4 and 20.5 km in altitude with 300-m range resolution, somewhat unevenly spaced in time (of the order of 1 hour apart) but with no significant gaps. Total times for Scenes 2 and 3 are 266 and 180 hours. Figure 1 shows the mean horizontal wind magnitude and direction calculated from the radar data, as well as the temperature profile averaged from balloon rawinsonde measurements made from San Juan (every 12 hours normally but specially arranged to be double the usual frequency during Scene 2). Plate 1 is a map of the residual velocities in the direction of 33° azimuth after the mean component from Figure 1 has been subtracted. As one would expect, there is a clear distinction in the dynamics below and above the tropopause (~ 17 km). Without any further analysis, one can already see wavelike activity above the tropopause with a distinctly down-

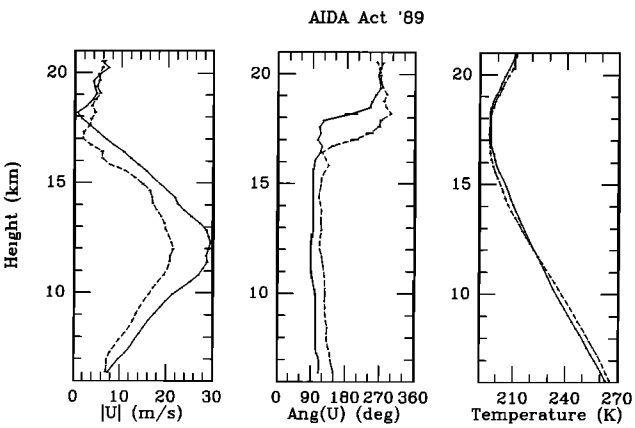

Figure 1. The mean horizontal (left) wind speed and (middle) direction measured by the Arecibo 430-MHz radar during AIDA Scene 2 (solid lines) and Scene 3 (dashed lines). The direction is the wind blowing toward the given angle, which is measured clockwise from 0° N. (right) The mean temperature profiles were measured by radiosondes launched on balloons from San Juan every 6 hours during Scene 2 (solid line) and every 12 hours during Scene 3 (dashed line). San Juan is approximately 80 km east of Arecibo.

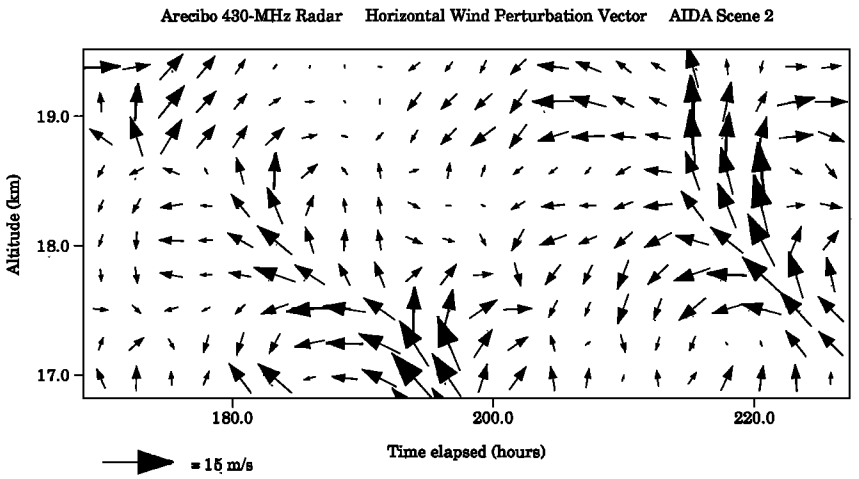

Figure 2. Horizontal perturbation wind vectors plotted for a selected time and altitude range of Scene 2. Up is north and right is east.

ward trend in the phase that is suggestive of upward propagating IGWs. The consistent downward phase propagation above the tropopause is even more clear in the Scene 3 data (see Plate 2).

In order to form the horizontal wind vector from the two orthogonal wind data or to apply FFT techniques, one must have evenly spaced data points. Thus we performed cubic spline-fit interpolations across time and resampled evenly. Note that the resulting data above $\sim$ 20 km and below $\sim$ 7 km are suspect due to gaps in the original data (see Plate 1 and Plate 2); therefore we will constrain further analysis in between those delimiters.

A quick look at the subsequent horizontal perturbation wind vectors shows that, indeed, the vectors tend to rotate clockwise with altitude and time in the region where wavelike activity is evident, giving further support for an IGW interpretation (see Figure 2).

The Cross Spectra

Let us now examine the autospectra and cross spectra of u and v. We will concentrate on the region around and above the tropopause. For Scene 2, the entire time-altitude data grid consists of 97 points in time spaced 2.77 hours apart and 49 points in altitude spaced 0.3 km apart. For Scene 3, the altitude grid is the same with 63 points in time spaced 2.86 hours apart. Figure 3 shows the autospectra and cross spectra taken with respect to time for the entire length of the Scene 2 data set and averaged across the region above the tropopause. The error bars are plus/minus twice the standard deviation divided by the square root of the number of averages, which represent the 95% confidence limits for the determination of the mean in a normal distribution. However, the distribution of the coherence and phase variables is not expected to be normal. *Jenkins and Watts* [1968] apply Fisher's z transformation to the coherence and a tangent function to the phase to obtain theoretical confidence intervals that are dependent on the value of the coherence and the smoothing factor. Using their results we get, for the case of Figure 3 and for $C_{UV} = 0.8$ and $\Phi_{UV} = 0°$, 95% confidence intervals of $0.71 < C_{UV} < 0.86$ and $-8.9° < \Phi_{UV} < 8.9°$. On the whole, our error bars are reasonably consistent with the theoretical expectations.

In Figure 3, one is immediately struck by the peaks in the autospectra and the coherence located between the local inertial frequency of 0.63 day^{-1} and the diurnal frequency. Clearly, there is coherent wave energy at those observed frequencies. However, one cannot draw firm conclusions regarding the intrinsic frequencies since the observed frequencies are Doppler shifted by the mean horizontal winds, which, during the 266 hours over which the spectra were taken, varied significantly. The phases corresponding to the peak coherence region are positive (CW rotation) and elliptic, suggestive of IGWs. In fact, the phase values are consistently positive and elliptic up to a transitional frequency of about 2 day^{-1} above which the phases tend toward $\pm 180°$. One could interpret this phase transition behavior as the vanishing of the Coriolis effect as the wave frequency becomes much greater than the inertial frequency; in other words, IGWs giving way to pure gravity waves with increasing frequency. The $\pm 180°$ trend suggests that the high-frequency waves were traveling toward the northwest or southeast quadrant. However, it must be noted that the phase error bars are quite large at the higher frequencies.

Next we examine the same time-altitude region by taking the spectra with respect to altitude and averaging with respect to time (see Figure 4). In this case, both the autospectral power and the cross-spectral coherence drop off with increasing wavenumber. There are no big peaks, but it is clear that the phase in the low wavenumber regime is positive (CW) and elliptic, which is indicative of upward propagating IGWs. Again, there appears to be a trend toward $\pm 180°$ at the higher wavenumbers, hinting at a transition to pure gravity waves, but the coherences at the highest wavenumbers are probably too low for us to draw a definite conclusion.

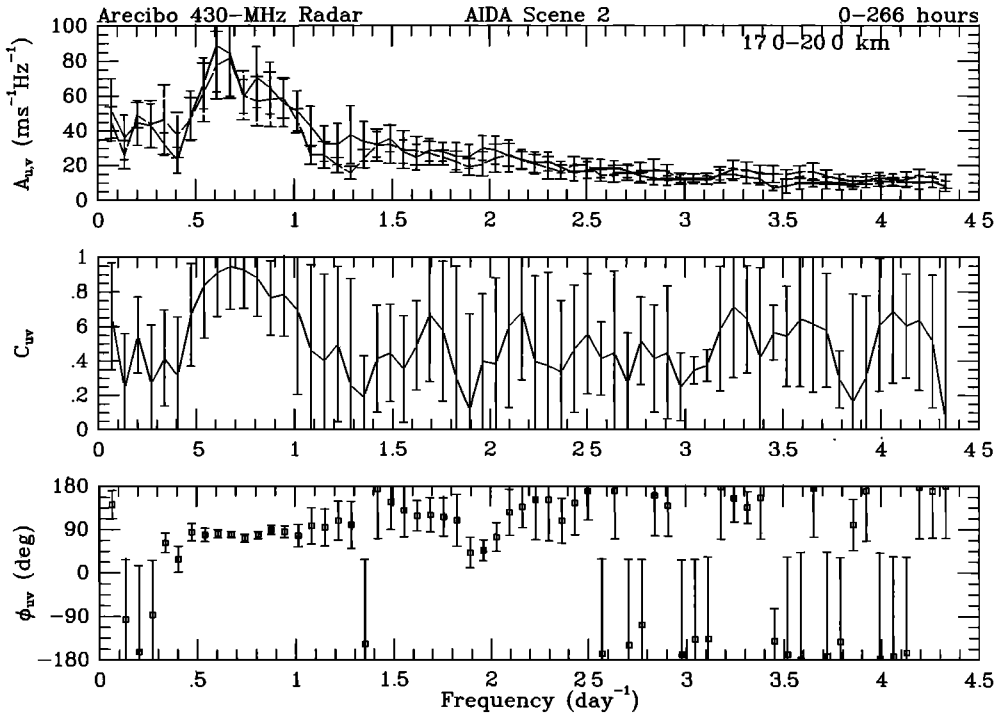

Figure 3. (top) The amplitudes of the autospectra of the zonal (solid line) and meridional (dashed line) perturbation velocities. The cross spectrum of the zonal and meridional components is shown as (middle) the coherence and (bottom) the phase. The spectra are taken with respect to time, and the cross spectrum is formed by averaging over altitude. The error bars are plus/minus twice the standard deviation divided by the square root of number of averages. The time interval and altitude range used are shown at the top right. The 0 hour corresponds to March 28, 1989, 2200 UT.

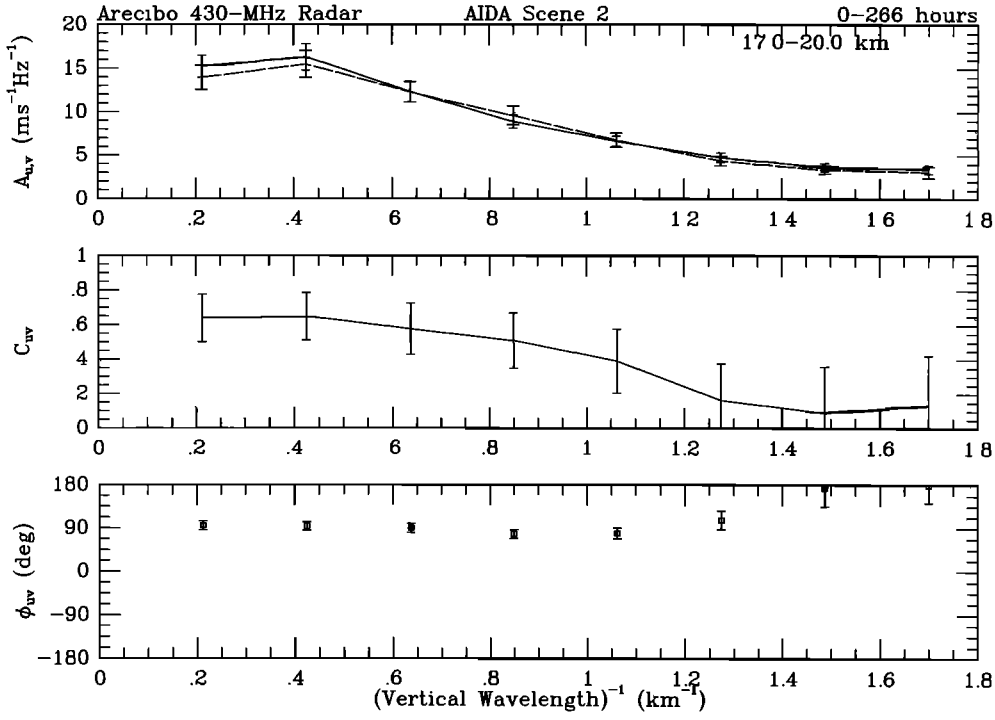

Figure 4. Same as Figure 3 except the spectra are taken with respect to altitude and the cross spectrum is formed by averaging over time.

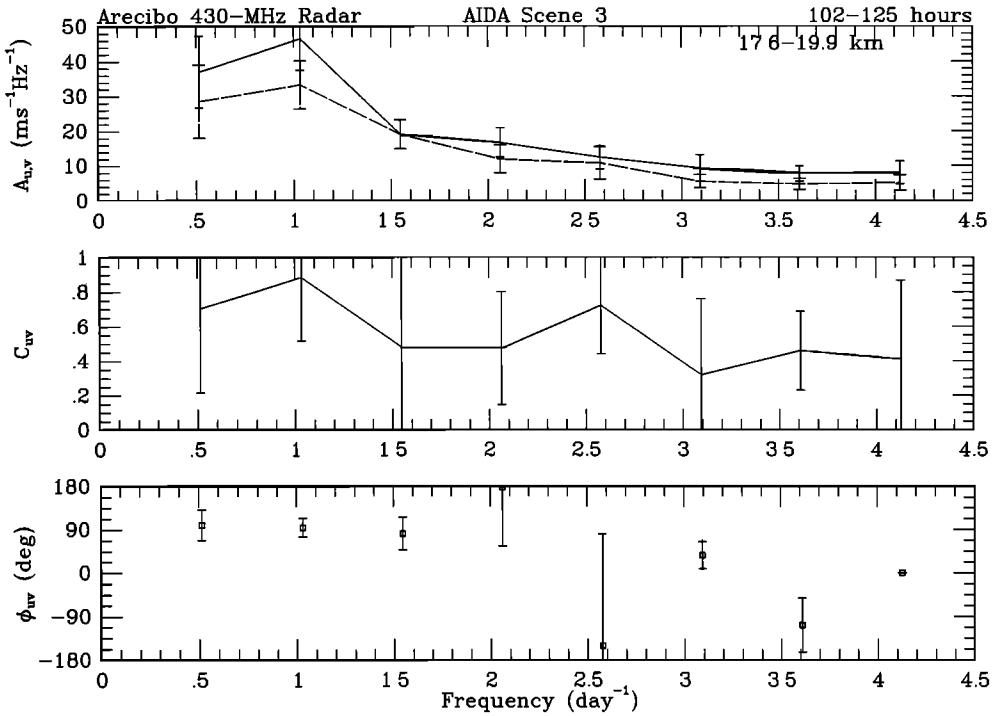

Figure 5. Same as Figure 3 except that the data are from Scene 3 with a shorter time period and a slightly different altitude range.

IGW Parameter Estimation

Note from (5) that the estimate of ω depends on the measured background parameters N and $\partial\bar{v}/\partial z$. Since the rest of the IGW parameter estimates depend on ω, they too are affected by the background conditions. Consequently, the parameter estimates should be taken over a time-altitude region in which the background temperature and wind profiles do not vary appreciably. Let us therefore take a limited time-altitude region of the data on which to apply the wave-parameter extraction.

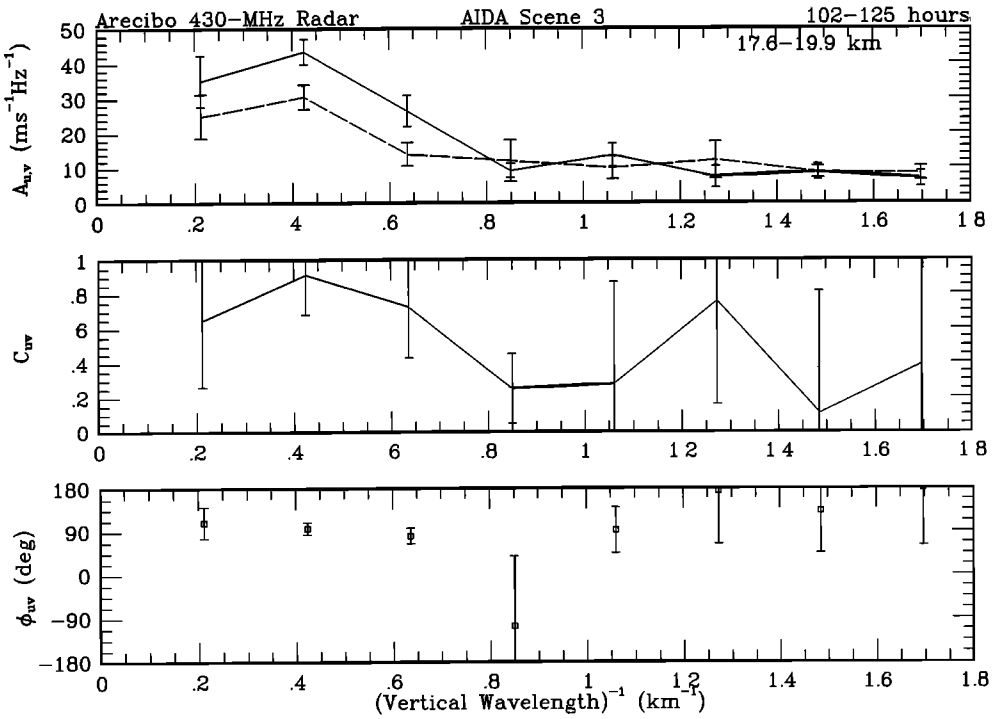

Figure 6. Same as Figure 5 except that the spectra are taken with respect to altitude and the cross spectrum is formed by averaging over time.

Figure 5 and Figure 6 show the autospectral and cross-spectral plots in the frequency and vertical wavenumber domains for the region 17.6–19.9 km in altitude and 102–125 hours in time of Scene 3, a region with a strong likelihood of containing IGW-like oscillations as seen from the velocity perturbation map (Plate 2). From Figure 5 we choose the frequency bin of 1.03 ± 0.26 day^{-1}, or $23^{+8}_{-4}\frac{2}{4}$ hours in terms of wave period, where the autospectra and coherence show clear maxima and the error estimate of the phase is low. From Figure 6 we choose the inverse vertical wavelength bin of 0.424 ± 0.106 km^{-1}, or $2.4^{+0}_{-0}\frac{74}{51}$ km in terms of wavelength, where the autospectra and coherence are at their highest and the phase error is at its lowest.

The application of the wave-parameter estimation method outlined in the previous section yields the values given in Table 1. Note that the uncertainties (plus/minus the standard deviation divided by the square root of the number of averages) from all the measured quantities have been propagated through the equations used to derive the wave parameters. The errors associated with the intrinsic period and horizontal propagation angle are reasonably small for both the ω-derived and the m-derived cases. This was true for other segments of the data on which we performed the wave parameter estimation procedure. For the rest of the parameters, the uncertainties in the m-derived quantities are smaller than those in the ω-derived values in Table 1. This was also true for other data segments analyzed and is likely due to the ω spectrum route requiring one more observable quantity ($\bar{u}$) and equation, (7). Finally, we note that it was very difficult to obtain a good estimate of the group velocities. Perhaps this is not surprising, since, as one can see from (9) and (10), they are dependent on so many of the other observed and derived parameters.

As for the measured background parameters, the Brunt-Väisälä frequency was very stable with small uncertainties. However, the transverse velocity gradient had rather large uncertainties, which we attribute to the errors in the angle of wave propagation (from which the transverse direction was determined) added on top of the difficulty in obtaining the derivative of data points with noise.

Table 1. Background Quantities and Inferred Inertio-gravity Wave (IGW) Parameters for Scene 3, Time: 101–125 hours; Height: 17.6–19.9 km

	Spectral Bin	
	$\frac{2\pi}{m} = 2.4$ km	$\frac{2\pi}{\omega_0} = 23$ hours
N^2, 10^{-4} rad^{2}s^{-2}	7.2 ± 0.12	7.2 ± 0.12
dV/dz, 10^{-4} s^{-1}	9.7 ± 6.2	11 ± 6.4
R	0.69 ± 0.051	0.71 ± 0.097
θ^a, deg	170 ± 7.4	170 ± 12
$2\pi/\omega$, hours	25 ± 1.9	26 ± 3.1
$2\pi/k$, km	1300 ± 170	310 ± 360
$2\pi/m$, km	...	0.55 ± 0.65
v_{gh}, m s^{-1}	7.5 ± 5.9	1.7 ± 43
v_{gz}, cm s^{-1}	1.4 ± 1.9	0.30 ± 42
v_{ph}, m s^{-1}	14 ± 2.0	3.3 ± 1.8
v_{pz}, cm s^{-1}	-2.6 ± 0.89	-0.58 ± 3.6

[a]Horizontal direction of wave propagation. Northward is 0° with increasing value in the clockwise sense.

Table 2. Background Quantities and Inferred Inertio-gravity Wave (IGW) Parameters for Scene 2, Time: 180–202 hours; Height: 17.6–19.9 km

	Spectral Bin	
	$\frac{2\pi}{m} = 2.4$ km	$\frac{2\pi}{\omega_0} = 22$ hours
N^2, 10^{-4} rad^{2}s^{-2}	7.2 ± 0.47	7.2 ± 0.47
dV/dz, 10^{-4} s^{-1}	2.8 ± 5.8	9.3 ± 7.9
R	0.57 ± 0.076	0.73 ± 0.14
θ^a, deg	-120 ± 7.7	130 ± 20
$2\pi/\omega$, hours	21 ± 2.4	27 ± 4.0
$2\pi/k$, km	940 ± 170	1100 ± 810
$2\pi/m$, km	...	1.8 ± 1.4
v_{gh}, m s^{-1}	8.3 ± 6.8	5.4 ± 110
v_{gz}, cm s^{-1}	2.1 ± 3.0	0.90 ± 86
v_{ph}, m s^{-1}	12 ± 2.3	11 ± 5.1
v_{pz}, cm s^{-1}	-3.1 ± 1.1	-1.8 ± 6.7

[a]Horizontal direction of wave propagation. Northward is 0° with increasing value in the clockwise sense.

In general, the wave parameters of Table 1 are in line with previous observations over Arecibo by *Maekawa et al.* [1984] and *Cornish and Larsen* [1989]. Also, the vertical phase descent of ~ -3 cm s^{-1}, which translates to ~ -3 km day^{-1}, is of the order of the velocity perturbation descent seen above the tropopause in Plate 2.

We analyzed other data segments as well. In particular, we show results from a segment from Scene 2 using the same criteria as used above to pick the frequency and wavenumber bins. The chosen frequency bin of 1.08 ± 0.27 day^{-1} (or $22^{+7}_{-4}\frac{6}{2}$ hours in terms of wave period) had $C_{UV} = 0.88 \pm 0.40$ and $\Phi_{UV} = 73° \pm 16°$, while the selected wavenumber bin of 0.424 ± 0.106 km^{-1} (or $2.4^{+0.74}_{-0.51}$ km in terms of wavelength) had $C_{UV} = 0.88 \pm 0.38$ and $\Phi_{UV} = 65° \pm 15°$. The results are listed in Table 2. The same comments apply as to Table 1. Again, the extracted vertical phase speed is commensurate to what the eye roughly sees descending in Plate 1.

We also examined the effects of varying the measured input quantities, N^2, $\partial\bar{v}/\partial z$, and R, on the inferred wave parameters, by changing the value of each input, one at a time, by certain percentages. We would like to point out three general trends observed from this exercise.

1. The calculated intrinsic period is extremely stable against variations in the background quantities; this can also be seen from the small uncertainty values for $2\pi/\omega$ in Tables 1 and 2.

2. The values calculated from the m spectra are much more stable against input changes than the output of the ω_0 spectra. This result is not unexpected, since the m spectra route requires the solution of only two equa-

tions with two unknowns, while the ω_0 spectra route has three equations with three unknowns. It boils down to the fact that a radar can measure the local vertical wavelength but can only observe the Doppler-shifted period of an IGW.

3. Variations in R, which is calculated from the observed wind perturbations, affect the output more than the background variations in the vertical shear and Brunt-Väisälä frequency. Therefore the major limitation in accuracy of IGW wave-parameter extraction results not from the variation of the background quantities (a weakness of the cross-spectral method) but from the determination of the wind perturbation vector ellipse, which is a problem for both the hodograph and the cross-spectral methods.

Summary Discussion

After outlining the cross-spectral technique, we demonstrated its usefulness in analyzing IGWs. The coherence of the cross spectrum between u and v is a paradigm for the presence of a geophysical wave in a given spectral bin, which is a piece of information not available from the autospectra of u and v. The cross-spectral phase yielded the ellipticity and sense of rotation of the horizontal velocity perturbation vector, which gave the vertical sense of wave energy propagation (in the case of spectra taken with respect to height) and revealed a transition from IGWs to pure gravity waves in the lower stratosphere at the semidiurnal period. Furthermore, the cross-spectral phase together with the autospectral amplitudes defined an ellipse for each spectral bin such that IGW parameters could be extracted, in the same way that the parameters are inferred from hodographs.

Further sensitivity tests showed that the intrinsic wave frequency, ω, is the most stable output parameter against variability in the inputs, not a surprising result since ω is directly calculated from the input quantities, whereas all the other output parameters depend on ω and/or other quantities. Another result of the sensitivity test was that wave parameters inferred from the vertical wavenumber spectra were more stable than those calculated from the frequency spectra, which was also not unexpected since the observed wave frequencies are Doppler shifted (thus introducing an additional variable), whereas the observed vertical wavenumbers can be taken as true values (in a local sense). Therefore, if possible, IGW parameters should be inferred from the vertical wavenumber spectra rather than the frequency spectra. Finally, the sensitivity tests showed that variability in the the background parameters is not likely to be the limiting factor in the accuracy of the inferred wave parameters (which had initially been suspected to be the major disadvantage of the cross-spectral method due to its need to take data from a larger time-altitude domain than the other methods). Rather, it is the variability in the horizontal perturbation wind ellipse that introduces the biggest fluctuations in the output parameters. Unfortunately, the variabilities are nonnegligible and place fairly large uncertainties on some of the inferred wave parameters. This problem applies equally well to the hodograph method; it is simply the problem of trying to infer so much information from a limited set of input variables.

As for the question of whether we are observing a real IGW over Arecibo or a mountain wave with background shears that make it appear to be an IGW, we believe that our analysis of Scenes 2 and 3 from AIDA makes a strong case for real IGWs in the lower stratosphere for the following reasons.

1. Plates 1 and 2 showed more clearly than in previous Arecibo data that long-period, short vertical-scale, horizontal velocity perturbations above the tropopause had consistently descending phase speeds.

2. Consistent rotation of the horizontal wind perturbation vector with respect to time (e.g., Figure 2) is a mark of an IGW but not of a quasi-stationary mountain wave.

3. The ellipticity introduced to the intrinsically linear polarization of a mountain-wave height hodograph is limited by $R \approx |N^{-1}dV/dz|$. For the cases of Table 1 and Table 2, we calculate that the quantity on the right-hand side of this equation is at least an order of magnitude smaller than the quantity on the left. Therefore we conclude that the background vertical shears were not great enough to account for the ellipticities observed.

4. The cross-spectral analysis of u and v showed that there was coincidence between high coherence and peaks in the autospectra between the local inertial frequency and the diurnal frequency, indicating the dominant presence of waves at the observed long periods.

Acknowledgments. The Arecibo Observatory is part of the National Astronomy and Ionosphere Center, which is operated by Cornell University under a cooperative agreement with the National Science Foundation. The San Juan radiosonde data were obtained from the National Center for Atmospheric Research Data Base, which is supported by the National Science Foundation. I would like to thank H. Mario Ierkic for taking the Arecibo ST radar data during AIDA, R. Alan Johnson for writing the spectral fitting subroutines, and Kaoru Sato for clarification regarding her dispersion relation.

References

Cornish, C. R., and M. F. Larsen, Observations of low-frequency inertia-gravity waves in the lower stratosphere over Arecibo, *J. Atmos. Sci.*, *46*, 2428–2439, 1989.

Cot, C., and J. Barat, Wave-turbulence interaction in the stratosphere: A case study, *J. Geophys. Res.*, *91*, 2749–2756, 1986.

Eckermann, S. D., and W. K. Hocking, The effect of superposition on measurements of atmospheric gravity waves: A cautionary note and some reinterpretations, *J. Geophys. Res.*, *94*, 6333–6339, 1989.

Eckermann, S. D., and R. A. Vincent, Falling sphere observations of anisotropic gravity wave motions in the upper stratosphere over Australia, *Pure Applied Geophys.*, *130*, 509–532, 1989.

Gonella, J., A rotary-component method for analysing meteorological and oceanographic vector time series, *Deep Sea Res.*, *19*, 833–846, 1972.

Hayashi, Y., Space-time spectral analysis of rotary vector series, *J. Atmos. Sci.*, *36*, 757–766, 1979.

Hines, C. O., Tropopausal mountain waves over Arecibo: A case study, *J. Atmos. Sci.*, *46*, 476–488, 1989.

Hines, C. O., G. W. Adams, J. W. Brosnahan, F. T. Djuth, M. P. Sulzer, C. A. Tepley, and J. S. Van Baelen, Multi-instrument observations of mesospheric motions over Arecibo: comparisons and interpretations, *J. Atmos. Terr. Phys.*, *55*, 241–287, 1993.

Jenkins, G. M., and D. G. Watts, *Spectral Analysis and Its Applications*, 523 pp., Holden-Day, Merrifield, Va., 1968.

Kundu, P. K., An analysis of inertial oscillations observed near Oregon coast, *J. Phys. Oceanogr.*, *6*, 879–893, 1976.

Kunze, E., Near-inertial wave propagation in geostrophic shear, *J. Phys. Oceanogr.*, *15*, 544–565, 1985.

Maekawa, Y., S. Fukao, T. Sato, S. Kato, and R. F. Woodman, Internal inertia-gravity waves in the tropical lower stratosphere observed by the Arecibo radar, *J. Atmos. Sci.*, *41*, 2539–2545, 1984.

Meriwether, J. W., Lidar observations of atmospheric dynamics in the troposphere and lower stratosphere over Arecibo, *J. Geophys. Res.*, *98*, 20,713–20,723, 1993.

Sato, K., A statistical study of the structure, saturation and sources of inertio-gravity waves in the lower stratosphere observed with the MU radar, *J. Atmos. Terr. Phys.*, *56*, 755–774, 1994.

Sato, K., and M. Yamada, Vertical structure of atmospheric gravity waves revealed by the wavelet analysis, *J. Geophys. Res.*, *99*, 20,623–20,631, 1994.

Sato, T., and R. F. Woodman, Spectral parameter estimation of CAT radar echoes in the presence of fading clutter, *Radio Sci.*, *17*, 817–826, 1982.

Thomas, L., I. T. Prichard, and I. Astin, Radar observations of an inertia-gravity wave in the troposphere and lower stratosphere, *Ann. Geophys.*, *10*, 690–697, 1992.

Thompson, R. O. R. Y., Observation of inertial waves in the stratosphere, *Q. J. R. Meteorol. Soc.*, *104*, 691–698, 1978.

Vincent, R. A., and D. C. Fritts, A climatology of gravity wave motions in the mesopause region at Adelaide, Australia, *J. Atmos. Sci.*, *44*, 748–760, 1987.

Woodman, R. F., High-altitude resolution stratospheric measurements with the Arecibo 430-MHz radar, *Radio Sci.*, *15*, 417–422, 1980.

J. Y. N. Cho, Arecibo Observatory, National Astronomy and Ionosphere Center, P.O. Box 995, Arecibo, PR 00613. (e-mail: jcho@naic.edu)

(Received September 9, 1994; revised April 12, 1995; accepted May 18, 1995.)